

# Failure Analysis of Coating Adhesion: Peeling of Internal Oxidation Layer over Electrical Steel after Stress Relief Annealing

HSIN-WEI LIN

New Materials Research & Development Department  
China Steel Corporation

Electrical Steel (ES) is commonly used in the production of power generators, motor cores and transformers. The internal stresses and strains of ES can be generated during the manufacturing processes, therefore, they need to be removed by stress relief annealing. However, several clients of China Steel (CSC) reported that the coatings were peeled-off after the heat treatment of the ES. To resolve the problems and decrease the defect rate, this work focused on the analysis of the peeled-off coatings morphology and the optimization of heating parameters. Several instruments such as a dual-beam focused ion beam system, energy dispersive spectrometer, glow discharge spectrometer and transmission electron microscope were used to characterize the microstructures of the peeled-off coatings and well-attached samples. The results showed that samples after heat treatment were composed of three layers of structure including coat, Internal Oxidation Zone (IOZ) and substrate. Surprisingly, the occurrence of cracks present in the interface between IOZ and substrate were found. When the IOZ was peeled from the substrate, there was no possibility that the coatings could still remain on the surface. Generally speaking, the peeled-off samples featured a thicker layer of IOZ, while, containing a high concentration of oxides in this region. With precise control of gas composition and soaking time in the annealing section, the defect rate of adhesion failure could be effectively eliminated.

**Keywords:** Electrical steel, Coat, Internal oxidation, Annealing, Adhesion

## 1. INTRODUCTION

Non-oriented Electrical Steels (ES) are widely used in the production of power generators, motor cores and transformers. Manufacturing processes such as bending, shearing, and punching are usually unavoidable, which lead to the generation of internal stresses and strains of ES. These defects, however, could cause a deterioration of the magnetic properties in the final products. In order to remove the residual stresses in the deformed parts, high temperature heat treatment is commonly applied<sup>(1-5)</sup>. Figure 1 is the illustration of the general heating profiles of most ES clients. In general, heat treatment of ES comprises of three major steps including burn-off, annealing and bluing. In the first step, laminations are subjected to an atmospheric burn-off furnace to remove the stamping oil and lubricant. This step is also known as a degreasing process, temperature ranging from 300°C to 450°C, soaking time ranging from 1 to 2 hours. Accordingly, laminations are further proceeded by a Stress Relief Annealing (SRA) step. In this stage, atmosphere, heating temperature, and soaking time need to be carefully controlled to prevent severe oxidation of the ES substrate. Dehu-

midified DX gas and HN gas are usually used as protective gas in the SRA process. Annealing temperature and soaking time could range from 650°C to 850°C and 1 to 2 hours, respectively, depending on the grade of the ES. During the SRA process, the internal stresses of deformed parts could be relieved by recrystallization, resulting in a recovery of core loss. Subsequently, laminations are slowly cooled to a temperature of 450°C ~550°C for the bluing process. This bluing treatment is performed by increasing the dew point of protective

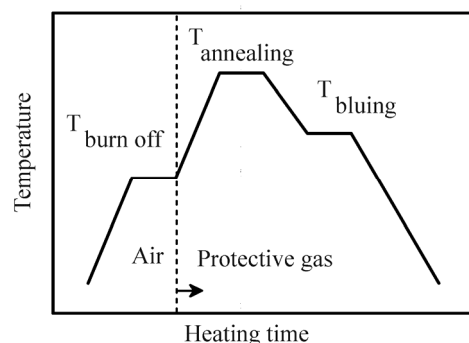


**Fig.1.** Illustration of general heating profile.

gas, which could form an insulation layer in the cut edge to prevent further rusting. Finally, laminations are transferred to a cooling chamber where they are brought down to handling temperature.

In China Steel (CSC), two major types of semi-inorganic coats are supplied, which are chromium (Cr)-containing C628 coat and Cr-free C6N8 coat<sup>(6-8)</sup>. These coats provide superior properties of ES such as interlayer resistance, punch-ability, weldability and corrosion resistance. Moreover, these coats could also withstand the SRA temperature, while maintain adequate interlayer resistance and coating adhesion after SRA. Recently, one of our customers responded that the quality of C6N8 coat showed a certain degree of discrepancy. The coating adhesion after SRA treatment was poor, which failed to pass the tape test in final inspection of the motor cores. Therefore, in this study, the microstructures of peeled-off and well-attached samples after SRA treatment were fully investigated. By several analyses, the results showed that adhesion failure occurred at the interface of ES substrate and internal oxide layer. The internal oxide layer was extrinsic, which was formed due to unappropriated annealing conditions. By precisely controlling the heating parameters, we were able to resolve the peeling-off problems and decrease the rate of defective ES.

## 2. EXPERIMENTAL METHOD

### 2.1 Information of heat-treated samples

In this study, two representative samples A and B, were collected from two different annealing lines of a ES customer. Sample A showed poor coating adhesion after heat treatment. The coats were severely peeled after the 3M scotch 600 tape test. The sampled atmosphere collected from the corresponding furnace contained a high percentage of oxygen. On the contrary, sample B showed good coating adhesion after the tape test. With no remarkable oxygen content detected in the corresponding sampled furnace atmosphere.

### 2.2 Analyzing methods and instruments

A Field Emission Scanning Electron Microscope (FE-SEM) equipped with Dual-Beam Focused Ion Beam (DB-FIB; model: FEI Helios Nanolab G3 CX) was used to prepare and observe the specimens for cross-sectional images. Scanning Ion Microscope (SIM) of DB-FIB and Transmission Electron Microscopy (TEM; model: JEOL JEM-2100) were also used to observe the cross-sectional morphologies. Elemental analyses and mapping were detected with an Energy Dispersive Spectrometer (EDS). The depth profiles of elemental distribution were analyzed with a Glow Discharge Spectrometer (GDS; model: RF GD Profiler HR).

## 3. RESULTS AND DISCUSSION

### 3.1 Mechanism of coat peeling

In order to realize the mechanism of coat peeling, tape tested sample A was first examined. Figure 2 demonstrates the SEM image of peeled-off sample A. From the top view of the sample surface, it can be clearly identified that the right hand side of the image was the bare ES substrate. The uncoated ES substrate should be flat with low surface roughness. However, after the heat treatment of the ES, a high degree of surface roughness of bare substrate was present. Due to high surface roughness, the peeled-off area showed a foggy white color to the naked eye. By selective etching of gallium ion, we were able to observe the cross-sectional region of sample A. Figure 3 demonstrates the cross-sectional images of SEM and SIM respectively. From the electron image, a small crack could be observed beneath the coat layer. However, by observing the contrast-enhanced ion image, we could further notice that the heat-treated ES was actually consist of three different layers of structure.

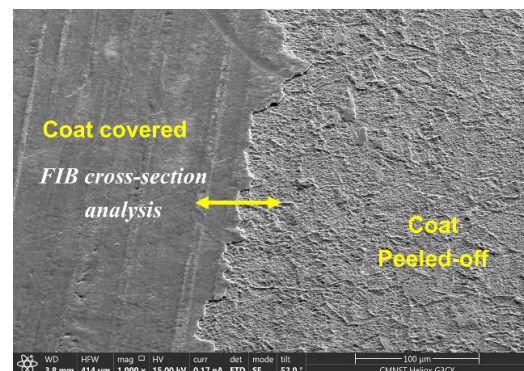
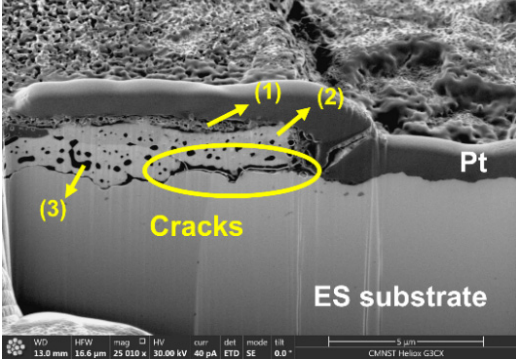
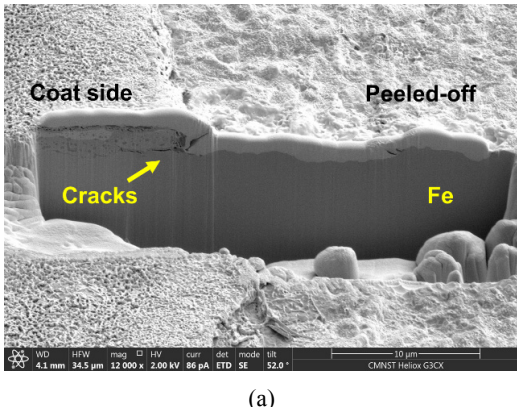


Fig.2. SEM top view images of peeled-off sample A.

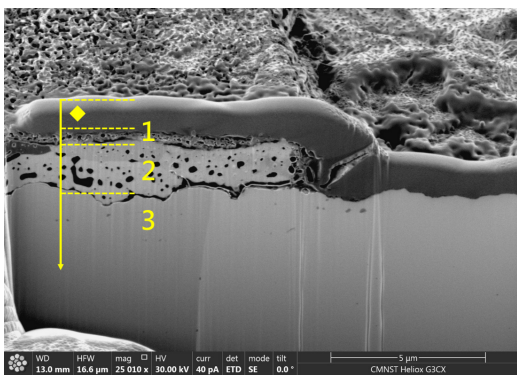
In order to understand the composition of each layer, the corresponding analysis of EDS is also provided in Table 1. Firstly, high concentrations of C, O and P were detected in the top layer, which suggested that this layer was the inherent CSC coat. After heat-treatment, the coat showed a porous structure with an average thickness of 0.5 um. It is worth to mention that the coat thickness before heat treatment was 0.7 um. Since the organic parts of the coat were decomposed during heat treatment, the shrinkage of thickness should be reasonable. Secondly, the middle layer was the Internal Oxidation Zone (IOZ), which formed during the heat treatment by the client. It could also be noticed that several particles, which were identified as black dots in SIM image, randomly located in the IOZ structure. The result of EDS showed that blank areas of the IOZ structure was mainly composed of Si and Fe.

**Table 1** Elemental analysis of the peeled-off sample determined by EDS

SIM cross-sectional image	Element (wt%)	Spot 1	Spot 2	Spot 3
	C	3.60	-	1.07
	O	10.98	-	6.76
	Al	1.33	-	2.54
	Si	3.24	1.06	6.08
	P	6.67	-	-
	Mn	2.21	-	1.42
	Fe	71.97	98.94	82.13



(a)



(b)

**Fig.3.** Cross-sectional images of peeled-off sample A. (a) SEM (magnification, 12,000×); (b) SIM (magnification, 25,010×).

However, the black dots are composed of high concentration of Si, Al and O, suggesting that these were the mixtures of silicon oxides and aluminum oxides<sup>(9)</sup>. Furthermore, these oxides were further aggregated into a continuous, worm-like structure, enriched at the bottom of the IOZ. Thirdly, the bottom layer is the original ES substrate, namely Si-Fe alloy. Unexpectedly, the cracks, which led to the occurrence of fracture, located

at the interface between the IOZ and ES substrate. It is suggested that the adhesion of these oxides and ES was poor. When the IOZ was peeled from the substrate, there was no possibility that the coats could still remain on the surface.

### 3.2 Characterizations of peeled-off and well-attached samples

To identify the characteristics of peeling morphology, two untested samples, peeled-off sample A and well-attached sample B, are thoroughly studied in this section. Figure 4 demonstrates the top view SEM images of sample A and B. After heat treatment, some cracks and pinholes were discovered on both surfaces. Since the coat contained polymer resins, the organic parts were eventually decomposed into volatile species. When these small molecules diffused out from the coat film, it could form the structure of cracks and pinholes. Generally speaking, two samples showed different morphologies. Sample A contained more cracks than sample B, however, sample B contained more pinholes than sample A. It may suggest that the decomposition rate of coats in two furnaces were slightly different.

Figure 5 shows the cross-sectional SIM images of untested sample A and B respectively. The result indicated that sample A contained much higher concentration of oxides than sample B. Moreover, the thickness of the IOZ of sample A was also thicker than sample B. Figure 6 presents the elemental depth profiles of sample A and B by GDS. With the assistance of cross-sectional images, the boundaries of each layer could be easily identified. The thicknesses of the first coat layer of the two samples were nearly identical. However, the second layers showed a great difference in elemental distribution. In sample A, it was found that such elements like Si, Al, Mn and O had a remarkable increment as compared to sample B. This result indicated that the concentration of oxides in sample A were

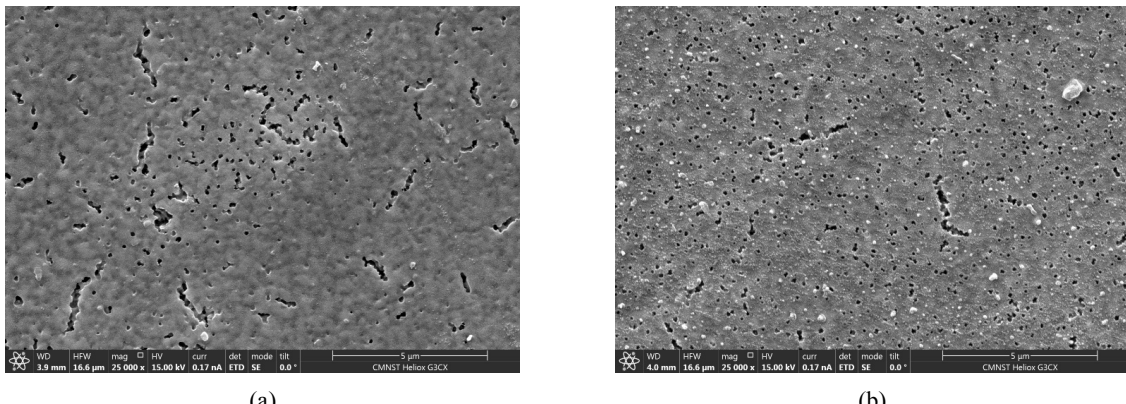


**Fig.4.** SEM top view images of untested (a) sample A and (b) sample B.

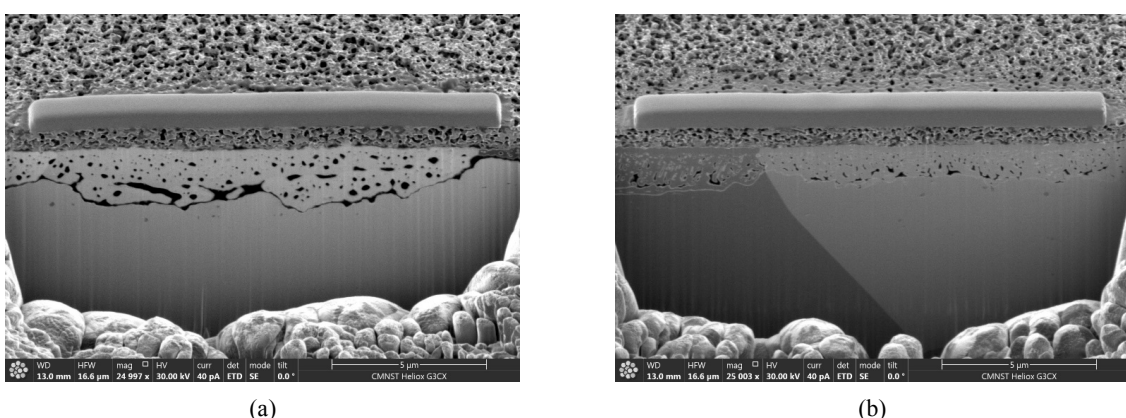


**Fig.5.** SIM cross-sectional images of (a) sample A and (b) sample B.

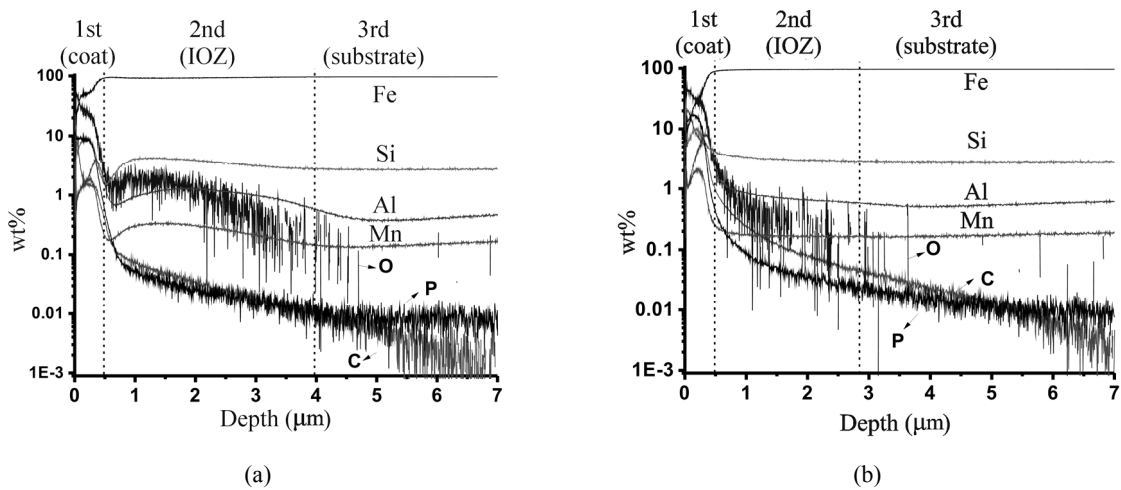


**Fig.6.** GDS depth profile analysis of (a) sample A and (b) sample B.

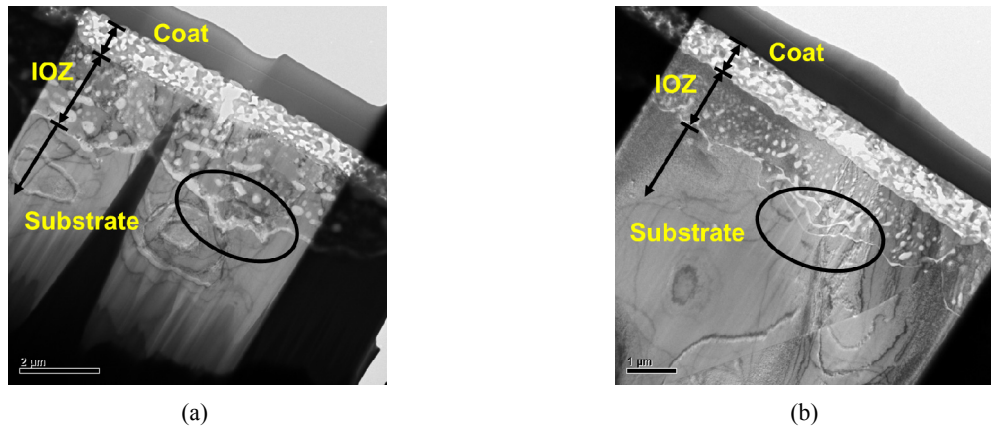
much higher than that in sample B, which was in agreement with the result of the cross-sectional image.

Figure 7 shows the TEM images of sample A and B. Likewise, three layers of structure could also be evidently observed. The circled areas revealed that the concentrated oxides were accumulated on the interface

between IOZ and substrate. These oxides could also be found in the well-attached sample B by observing with a high resolution TEM. However, the thickness of these oxides were relatively thin as compared to that in sample A. Figure 8 shows the corresponding EDS mapping results of TEM images. The results were consistent

with the EDS analyses in Table 1. Particles and worm-like structure in the IOZ were mainly formed with Si, Al and O, which proved that they were mixtures of silicon oxides and aluminum oxides. Interestingly, the results of mapping further suggested that dispersed particles were primarily formed with silicon oxide, and the worm-like oxides in the interface were

majorly formed with aluminum oxides. Since Si and Al were the active elements in ES alloy, the segregation of Si and Al at the grain boundary during heat treatment would be inevitable. As contacting low partial pressure of oxygen, Si and Al could be oxidized first rather than Fe due to the reactivity. Therefore, it led to the formation of silicon oxides and aluminum oxides, instead



**Fig.7.** TEM cross-sectional images of (a) sample A and (b) sample B.

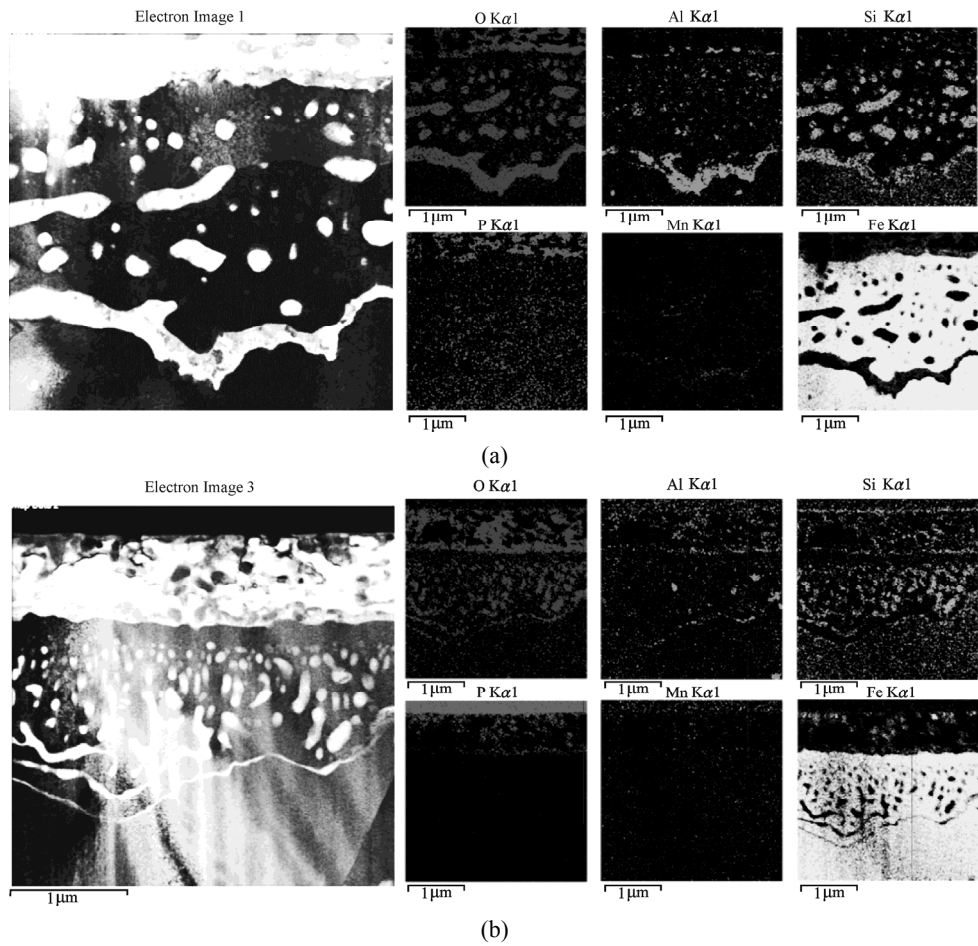


**Fig.8.** EDS mapping of sample A and sample B.

of magnetite ( $\text{Fe}_3\text{O}_4$ ) and hematite ( $\text{Fe}_2\text{O}_3$ ). According to the references<sup>(10)</sup>, these oxides had lower coefficients of thermal expansion than iron. Significant stresses could be generated in the interfaces during the heat treatment, which accelerated the occurrences of peeling accordingly.

### 3.3 Optimization of Heating parameters

Since the segregation of Si and Al were thermodynamically controlled, it might be possible to adjust the heating parameters to avoid the enormous peeling of IOZ. In order to clarify the effects of heating parameters on peeling, four different heating profiles were tested in this study. In Table 2, the results suggested that gas composition had a minor effect on the IOZ peeling, however, soaking time showed a major influence on it. By altering the soaking time in the annealing section, the phenomenon of peeling could be easily noticed. Figure 9 offers the corresponding cross-sectional SIM images obtained with different heating profiles. The results indicated that the formation of IOZ and worm-like oxides could be strongly related with heating parameters. In the end, this work underscored the importance of heat treatment conditions of end users. With a circumspect control of annealing environment, the adhesion failure of IOZ could be eliminated.

## 4. CONCLUSIONS

In conclusion, the failure analysis of coating adhesion after ES heat treatment and the corresponding solution to prevent coat peeling are thoroughly discussed in this paper. Five key points can be summarized as followed:

(1) Peeled-off sample was first observed with SEM cross-sectional image. The result implied that the heat-treated sample was composed of three layers of structure, namely coat layer, IOZ layer and substrate layer.

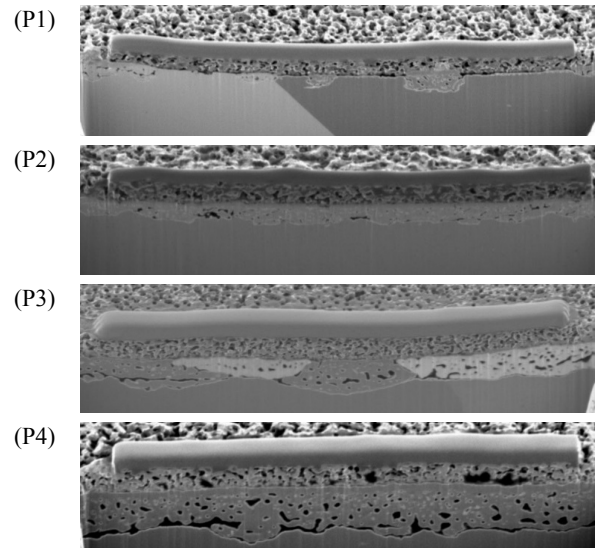


**Fig.9.** SIM cross-sectional images of samples obtained by different heat profiles.

- (2) Surprisingly, the occurrence of cracks present in the interface between IOZ layer and substrate layer. When the IOZ was peeled from substrate, there is no possibility that the coats could still remain on the surface.
- (3) Other instruments such as EDS, GDS and TEM were also used in order to clarify the microstructures of peeled-off and well-attached samples.
- (4) The peeled-off sample was characterized by the thickness of the IOZ, while, containing a high concentration of oxides in the IOZ region.
- (5) These oxides were mainly formed due to an unsuitable heat treating environment. By altering gas composition and soaking time in the annealing section, the defect rate of adhesion failure could be effectively eliminated.

**Table 2** The influence of heating parameters on the peeling of IOZ

Profile	SRA parameters		Tape test result <sup>c</sup>
	Gas composition <sup>a</sup>	Soaking time <sup>b</sup>	
P1	G1	S1	◎
P2	G2	S1	○
P3	G2	S2	X
P4	G2	S3	X

<sup>a</sup> G2 gas present higher oxygen contain than G1 gas.

<sup>b</sup> Soaking time: S1 < S2 < S3.

<sup>c</sup> Evaluation of adhesion: excellent ◎; good ○; poor X.

## REFERENCES

1. W. F. Block and N. Jayaraman: *J. Mater. Sci. Technol.*, 1986, vol. 2, pp. 22-27.
2. E. J. Hilinski and G. H. Johnston: "Annealing of Electrical Steel" in Electric Drives Production Conference, Nuremberg, Germany, 2014.
3. J. S. Park and J. T. Park: "Effect of Stress Relief Annealing Temperature and Atmosphere on the Microstructure and Magnetic Properties of Non-oriented Electrical Steels" in Electric Drives Production Conference, Nuremberg, Germany, 2016.
4. G. Lyudkovsky, A. G. Preban and J. M. Shapiro: *J. Appl. Phys.*, 1982, vol. 53, pp. 2419-2421.
5. S. C. Paolinelli and M. A. da Cunha: *J. Magn. Magn. Mater.*, 2006, vol. 304, pp. e599-e601.
6. J. C. Wu, P. C. Sun and P. L. Chen: China Steel Technical Report, 2008, No. 21, pp. 38-44.
7. K. Y. Peng, K. C. Hsieh, R. M. Chen and Y. P. Sui: China Steel Technical Report, 2012, No. 25, pp. 42-50.
8. C. K. Kuo and J. C. Wu: China Steel Technical Report, 2010, No. 23, pp. 46-51.
9. K. Yanagihara and S. Yamazaki: Nippon Steel Technical Report, 2011, No. 100, pp. 27-32.
10. L. L. Liu, Q. Q. Guo, S. Liu, C. S. Ni and Y. Niu: *Corros. Sci.*, 2015, vol. 98, pp. 507-515. □